Applied Mathematical Modelling 73 (2019) 95–108

Contents lists available at ScienceDirect

Applied Mathematical Modelling

journal homepage: www.elsevier.com/locate/apm

# Stress intensity factor for multiple cracks in bonded dissimilar materials using hypersingular integral equations

K.B. Hamzah[a,d], N.M.A. Nik Long[a,b,*], N. Senu[a,b], Z.K. Eshkuvatov[c]

[a] Laboratory of Computational Sciences and Mathematical Physics, Institute for Mathematical Research, Universiti Putra Malaysia, Serdang, Selangor 43400, Malaysia
[b] Mathematics Department, Faculty of Science, Universiti Putra Malaysia, Serdang, Selangor 43400, Malaysia
[c] Faculty of Science and Technology, Universiti Sains Islam Malaysia, Negeri Sembilan 71800, Malaysia
[d] Fakulti Teknologi Kejuruteraan Mekanikal dan Pembuatan, Universiti Teknikal Malaysia Melaka, Hang Tuah Jaya, Durian Tunggal, Melaka 76100, Malaysia

ARTICLE INFO

*Article history:*
Received 30 July 2018
Revised 26 February 2019
Accepted 1 April 2019
Available online 8 April 2019

*Keywords:*
Multiple cracks
Dissimilar materials
Hypersingular integral equation
Stress intensity factors

ABSTRACT

This paper deals with the multiple inclined or circular arc cracks in the upper half of bonded dissimilar materials subjected to shear stress. Using the complex variable function method, and with the help of the continuity conditions of the traction and displacement, the problem is formulated into the hypersingular integral equation (HSIE) with the crack opening displacement function as the unknown and the tractions along the crack as the right term. The obtained HSIE are solved numerically by utilising the appropriate quadrature formulas. Numerical results for multiple inclined or circular arc cracks problems in the upper half of bonded dissimilar materials are presented. It is found that the nondimensional stress intensity factors at the crack tips strongly depends on the elastic constants ratio, crack geometries, the distance between each crack and the distance between the crack and boundary.



## 1. Introduction

The emergence of cracks jeopardises the strength, hence makes failures or reduce the service life of materials and structures. The investigations of the related problems have resulted in a considerable number of research works, both theoretical and experimental, treating various type of cracks and materials encountered in practice. The mathematical modelling and formulation for cracks problems subjected to remote stress have been treated by many authors; in infinite plane [1–4], in half plane [5–9] and in bonded dissimilar materials [10–14].

Chen [10] calculated the nondimensional stress intensity factor (SIF) for two inclined cracks in the upper half of bonded dissimilar materials subjected to shear stress by using Fredholm integral equations with density distributions as an undetermined function. A logarithmic singular integral equation was formulated by using the complex potential method to solve a circular arc crack problem in the upper half of bonded dissimilar materials [11]. The continuous distributions of the body force along the cracks were used in finding the solution of an arbitrary array of cracks subjected to remote tension and

* Corresponding author at: Laboratory of Computational Sciences and Mathematical Physics, Institute for Mathematical Research, Universiti Putra Malaysia, Serdang, Selangor 43400, Malaysia.
*E-mail addresses:* khairum@utem.edu.my (K.B. Hamzah), nmasri@upm.edu.my (N.M.A. Nik Long), norazak@upm.edu.my (N. Senu), zainidin@usim.edu.my (Z.K. Eshkuvatov).

https://doi.org/10.1016/j.apm.2019.04.002
0307-904X/

shear, excluding the cracks at the interface [12] and including the crack at the interface [13] in bonded dissimilar materials. The complex stress function was used to investigate the accuracy of the stress intensity debonding fracture of bonded dissimilar materials [14]. The proportional crack opening displacements were used in obtaining the SIF for two-dimensional interface cracks, three-dimensional penny-shaped cracks and circumferential surface cracks in bonded dissimilar materials [15]. The interface cracks in bonded dissimilar materials was formulated using complex variable techniques by considering the interfacial crack fields and singularities at dissimilar materials interfaces [16]. The boundary element method and the extended finite element method were used to analyze the linear elastic fracture of the interface cracks problems in bonded dissimilar materials [17]. Li and Viola [18] described the analytical solution of the finite central straight crack along the plane interface between two bonded dissimilar materials based on the complex potential technique. The effect of Poisson's ratio on the SIF for interface crack in bonded dissimilar materials was investigated by Ghajar et al. [19]. SIF for the collinear interface cracks between bonded dissimilar materials was calculated by combining two solutions which were the solution for the inner and the outer collinear cracks [20]. Mousavi and Aliha [21] numerically investigated the fracture parameters of a center interface crack in bonded dissimilar materials subjected to biaxial tensile loading by using finite element over deterministic method. The effect of interaction between an interfacial main crack and a subinterfacial microcrack in bonded dissimilar materials was analyzed by using finite element method [22]. Complex variable function method was used to solve the crack problems in bonded dissimilar materials [23–25].

In this paper, we formulate the cracks problems in bonded dissimilar materials subjected to remote stress in terms of hypersingular integral equations (HSIEs). Numerical results are presented to exhibit the efficiency and accuracy of the current method.

## 2. Problem formulation

Fundamental equations of complex variable function method can be found in Muskhelishvili [26]. The stress components ($\sigma_x$, $\sigma_y$, $\sigma_{xy}$), the resultant force function $f$ with components $X$ and $Y$, and the displacements ($u$, $v$) are related to the complex potential functions $\Phi(z)=\phi'(z)$ and $\Psi(z)=\psi'(z)$ as follows:

$$\begin{aligned}\sigma_x+\sigma_y &= 4Re\phi'(z)\\ \sigma_y-i\sigma_{xy} &= 2Re\phi'(z)+z\overline{\phi''(z)}+\overline{\psi'(z)}\\ \sigma_y-\sigma_x+2i\sigma_{xy} &= 2[\bar{z}\Phi'(z)+\Psi(z)]\end{aligned} \tag{1}$$

$$f=-Y+iX=\phi(z)+z\overline{\phi'(z)}+\overline{\psi(z)} \tag{2}$$

$$2G(u+iv)=\kappa\phi(z)-z\overline{\phi'(z)}-\overline{\psi(z)} \tag{3}$$

where $G$ is shear modulus of elasticity, $\kappa=3-4\nu$ for plane strain, $\kappa=(3-\nu)/(1+\nu)$ for plane stress and $\nu$ is Poisson's ratio and a bar over a function denotes the conjugated value. A derivative in a specified direction (DISD) is defined for two analytic functions $f(z)$ and $g(z)$, as follows

$$\frac{d}{dz}\{f(z)\overline{g(z)}\}=f'(z)\overline{g(z)}+f(z)\overline{g'(z)}\frac{d\bar{z}}{dz}. \tag{4}$$

Applying (4) into Eq. (2) yields

$$J(z)=\frac{d}{dz}\{-Y+iX\}=\phi'(z)+\overline{\phi'(z)}+\frac{d\bar{z}}{dz}\left[z\overline{\phi''(z)}+\overline{\psi'(z)}\right]=N+iT \tag{5}$$

where $J$ denotes the traction along the segment $\overline{z,z+dz}$ with its normal and tangential components are $N$ and $T$, respectively.

Complex potentials for the crack $L$ in an infinite plane modelled by the distribution of crack opening displacement (COD) function $g(t)$ can be expressed by Aridi et al. [27]

$$\phi(z)=\frac{1}{2\pi}\int_L\frac{g(t)dt}{t-z},\ \psi(z)=\frac{1}{2\pi}\int_L\frac{\overline{g(t)}dt}{t-z}+\frac{1}{2\pi}\int_L g(t)\left(\frac{d\bar{t}}{t-z}-\frac{\bar{t}dt}{(t-z)^2}\right) \tag{6}$$

where $g(t)$ is defined by

$$g(t)=\frac{2G}{i(\kappa+1)}\left[(u(t)+iv(t))^+-(u(t)+iv(t))^-\right], \tag{7}$$

$(u(t)+iv(t))^+$ and $(u(t)+iv(t))^-$ denote the displacements at point $t$ of the upper and lower crack faces, respectively.

For cracks in bonded dissimilar materials, we apply the modified complex potentials (MCP) of the form [11]:

$$\phi_1(z)=\phi_{1p}(z)+\phi_{1c}(z),\quad \psi_1(z)=\psi_{1p}(z)+\psi_{1c}(z) \tag{8}$$

where $\phi_{1p}(z)$ and $\psi_{1p}(z)$ are the principal parts and $\phi_{1c}(z)$ and $\psi_{1c}(z)$ are the complementary parts of complex potentials. The complex potentials for the lower plane are $\phi_2(z)$ and $\psi_2(z)$. The traction and displacement continuity conditions are

$$\left[\phi_1(t)+t\overline{\phi_1'(t)}+\overline{\psi_1(t)}\right]^+=\left[\phi_2(t)+t\overline{\phi_2'(t)}+\overline{\psi_2(t)}\right]^-,\ t\in L \tag{9}$$

$$G_2\left[\kappa_1\phi_1(t)-t\overline{\phi_1'(t)}-\overline{\psi_1(t)}\right]^+=G_1\left[\kappa_2\phi_2(t)-t\overline{\phi_2'(t)}-\overline{\psi_2(t)}\right]^-,\ t\in L \tag{10}$$

Applying Eq. (8) into Eqs. (9) and (10), the following expressions are obtainable:

$$\begin{aligned}
\phi_{1c}(z)&=\beta_1\left[z\overline{\phi_{1p}'}(z)+\overline{\psi_{1p}}(z)\right]\\
\psi_{1c}(z)&=\beta_2\overline{\phi_{1p}}(z)-\beta_1\left[z\overline{\phi_{1p}'}(z)+z^2\overline{\phi_{1p}''}(z)+z\overline{\psi_{1p}'}(z)\right]\\
\phi_2(z)&=\left(1+\beta_2\right)\phi_{1p}(z)\\
\psi_2(z)&=\left(\beta_1-\beta_2\right)z\phi_{1p}'(z)+\left(1+\beta_1\right)\psi_{1p}
\end{aligned} \tag{11}$$

where $\overline{\phi_{1p}}(z)=\overline{\phi_{1p}(\bar{z})}$, and $\beta_1$, $\beta_2$ are bi-elastic constants defined as

$$\beta_1=\frac{G_2-G_1}{G_1+\kappa_1G_2},\quad \beta_2=\frac{\kappa_1G_2-\kappa_2G_1}{G_2+\kappa_2G_1}.$$

For a crack in the upper half of bonded dissimilar materials, applying Eq. (6) into (5) and letting point $z$ approaches $t_0$ on the crack and changing $d\bar{z}/dz$ into $d\bar{t}_0/dt_0$, yields the principal part of the traction as follow

$$(N(t_0)+iT(t_0))_{1p}=\frac{1}{\pi}\Xint-_L\frac{g(t)dt}{(t-t_0)^2}+\frac{1}{2\pi}\int_L A_1(t,t_0)g(t)dt+\frac{1}{2\pi}\int_L A_2(t,t_0)\overline{g(t)}dt \tag{12}$$

where

$$\begin{aligned}
A_1(t,t_0)&=\frac{1}{(t-t_0)^2}\left[\frac{(t-t_0)^2}{(\bar{t}-\bar{t}_0)^2}\frac{d\bar{t}}{dt}\frac{d\bar{t}_0}{dt_0}-1\right]\\
A_2(t,t_0)&=\frac{t-t_0}{(\bar{t}-\bar{t}_0)^3}\left[\frac{(\bar{t}-\bar{t}_0)}{(t-t_0)}\left(\frac{d\bar{t}}{dt}+\frac{d\bar{t}_0}{dt_0}\right)-2\frac{d\bar{t}}{dt}\frac{d\bar{t}_0}{dt_0}\right].
\end{aligned}$$

For the complementary part, substituting Eq. (11) into (5) and applying (6), and letting the point $z$ approaches $t_0$ on the crack and changing $d\bar{z}/dz$ by $d\bar{t}_0/dt_0$ gives

$$(N(t_0)+iT(t_0))_{1c}=\frac{1}{2\pi}\int_L\left(B_1(t,t_0)+B_2(t,t_0)\frac{d\bar{t}}{dt}\right)g(t)dt+\frac{1}{2\pi}\int_L\left(B_2(t,t_0)+B_3(t,t_0)\frac{d\bar{t}}{dt}\right)\overline{g(t)}dt \tag{13}$$

where

$$\begin{aligned}
B_1(t,t_0)&=\beta_1\left[\frac{1}{(t-\bar{t}_0)^2}+\frac{2(\bar{t}_0-\bar{t})}{(t-\bar{t}_0)^3}+\frac{d\bar{t}_0}{dt_0}\left(\frac{2(2t_0-3\bar{t}_0+\bar{t})}{(t-\bar{t}_0)^3}-\frac{6(\bar{t}_0-\bar{t})(\bar{t}_0-t_0)}{(t-\bar{t}_0)^4}-\frac{1}{(t-\bar{t}_0)^2}\right)\right]+\beta_2\frac{d\bar{t}_0}{dt_0}\frac{1}{(t-\bar{t}_0)^2}\\
B_2(t,t_0)&=\beta_1\left[\frac{1}{(\bar{t}-t_0)^2}+\frac{1}{(t-\bar{t}_0)^2}+\frac{d\bar{t}_0}{dt_0}\left(-\frac{1}{(t-\bar{t}_0)^2}-\frac{2(\bar{t}_0-t_0)}{(t-\bar{t}_0)^3}\right)\right]\\
B_3(t,t_0)&=\beta_1\left(\frac{1}{(\bar{t}-t_0)^2}+\frac{2(t_0-t)}{(\bar{t}-t_0)^3}\right).
\end{aligned}$$

Combining the principle (12) and complementary (13) parts of complex potentials, we obtain the HSIE for a crack in the upper half of bonded dissimilar materials as follows

$$(N(t_0)+iT(t_0))=\frac{1}{\pi}\Xint-_L\frac{g(t)dt}{(t-t_0)^2}+\frac{1}{2\pi}\int_L D_1(t,t_0)g(t)dt+\frac{1}{2\pi}\int_L D_2(t,t_0)\overline{g(t)}dt \tag{14}$$

where

$$\begin{aligned}
D_1(t,t_0)&=A_1(t,t_0)+B_1(t,t_0)+B_2(t,t_0)\frac{d\bar{t}}{dt}\\
D_2(t,t_0)&=A_2(t,t_0)+B_2(t,t_0)+B_3(t,t_0)\frac{d\bar{t}}{dt}.
\end{aligned}$$

Now consider two cracks $L_1$ and $L_2$ in the upper half of bonded dissimilar materials with remote tension $\sigma_x^\infty=p$ (Fig. 1(a)). By applying the superposition principle with the summation of an elastic bonded dissimilar materials with remote tension $\sigma_x^\infty=p$ (Fig. 1(b)), crack problems with loading on the crack faces of $L_1$ (Fig. 1(c)) and $L_2$ (Fig. 1(d)) we obtain

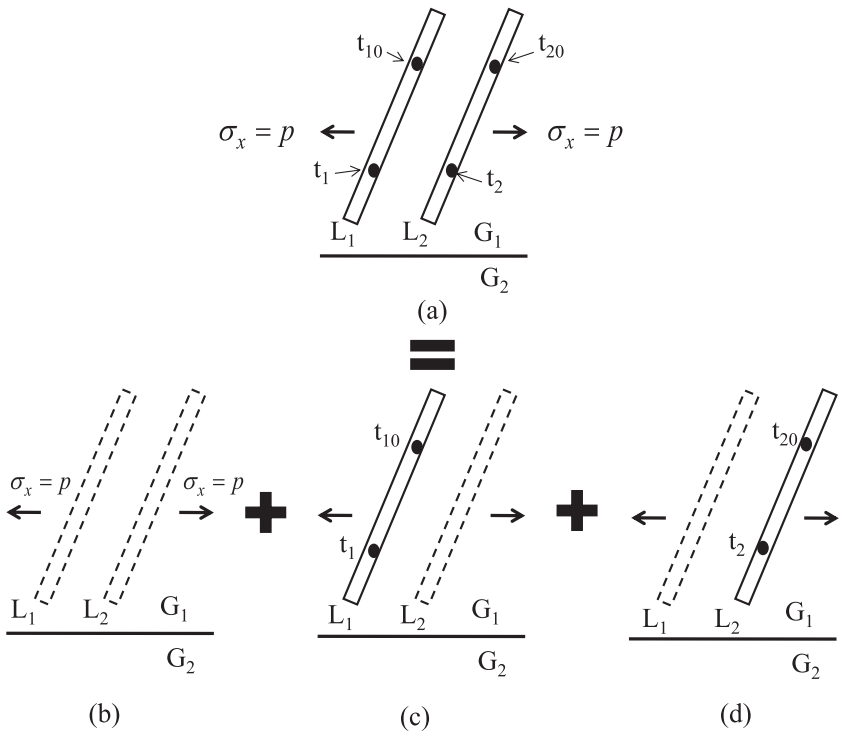


**Fig. 1.** Principle of superposition for the solution of two cracks problem in bonded dissimilar materials.

the HSIE for two cracks as

$$\begin{aligned}(N(t_{j0})+iT(t_{j0}))_j=&\frac{1}{\pi}\oint_{L_j}\frac{g_j(t_j)dt_j}{(t_j-t_{j0})^2}+\frac{1}{2\pi}\int_{L_j}D_1(t_j,t_{j0})g_j(t_j)dt_j\\&+\frac{1}{2\pi}\int_{L_j}D_2(t_j,t_{j0})\overline{g_j(t_j)}dt_j+\frac{1}{\pi}\int_{L_k}\frac{g_k(t_k)dt_k}{(t_k-t_{j0})^2}\\&+\frac{1}{2\pi}\int_{L_k}D_1(t_k,t_{j0})g_k(t_k)dt_k+\frac{1}{2\pi}\int_{L_k}D_2(t_k,t_{j0})\overline{g_k(t_k)}dt_k\end{aligned}\tag{15}$$

where $j,k=1,2$ $(j\neq k)$ and

$$\begin{aligned}D_1(t_j,t_{j0})&=A_1(t_j,t_{j0})+B_1(t_j,t_{j0})+B_2(t_j,t_{j0})\frac{d\bar{t}_j}{dt_j}\\D_2(t_j,t_{j0})&=A_2(t_j,t_{j0})+B_2(t_j,t_{j0})+B_3(t_j,t_{j0})\frac{d\bar{t}_j}{dt_j}\\D_1(t_k,t_{j0})&=A_1(t_k,t_{j0})+B_1(t_k,t_{j0})+B_2(t_k,t_{j0})\frac{d\bar{t}_k}{dt_k}\\D_2(t_k,t_{j0})&=A_2(t_k,t_{j0})+B_2(t_k,t_{j0})+B_3(t_k,t_{j0})\frac{d\bar{t}_k}{dt_k}.\end{aligned}$$

In Eq. (15), the first three integrals on the right hand side represent the traction influence on crack $L_1$ caused by COD $g_1(t_1)$ on crack $L_1$. The next three integrals represent the traction influence on crack $L_1$ caused by COD $g_2(t_2)$ on crack $L_2$.

If $G_2=0$, then $\beta_1=\beta_2=-1$, Eqs. (14) and (15) reduce to the HSIEs for the single and multiple cracks in a half plane elasticity [5], respectively. If $G_1=G_2$, then $\beta_1=\beta_2=0$, Eqs. (14) and (15) reduce to the HSIEs for the single and multiple cracks in an infinite plane [28], respectively.

In order to solve the HSIEs (14) and (15), we map the function $g_j(t_j)$ on a real axis $s$ with an interval $2a$ as follows:

$$g_j(t_j)|_{t_j=s_j}=\sqrt{a_j^2-s_j^2}H_j(s_j),\ j=1,2.\tag{16}$$

The HSIEs (14) and (15) together with (16) can be solved numerically by using the following quadrature formulas [2]

$$\frac{1}{\pi}\oint_{-a_j}^{a_j}\frac{\sqrt{a_j^2-s_j^2}H_j(s_j)ds_j}{(s_j-s_{j0})^2}=\sum_{j=1}^{M+1}W_j(s_{j0})H_j(s_j),\quad j=1,2 \tag{17}$$

$$\frac{1}{\pi}\int_{-a_j}^{a_j}\sqrt{a_j^2-s_j^2}H_j(s_j)ds_j=\frac{1}{M+2}\sum_{j=1}^{M+1}(a_j^2-s_{j0}^2)H_j(s_j),\quad j=1,2 \tag{18}$$

where $H_j(s_j)=H_{j1}(s_j)+iH_{j2}(s_j)$, $M\in\mathbb{Z}^+$,

$$s_{k,j}=a_k\cos\left(\frac{j\pi}{M+2}\right),\quad j=1,2,\ldots,M+1$$

and

$$W_j(s_{j0})=-\frac{2}{M+2}\sum_{n=0}^{M}(n+1)\sin\left(\frac{j\pi}{M+2}\right)\sin\left(\frac{(n+1)j\pi}{M+2}\right)U_n\left(\frac{s_{j0}}{a}\right)$$

and the observation points

$$s_{j0}=s_{j0,k}=a\cos\left(\frac{k\pi}{M+2}\right),\quad k=1,2,\ldots,M+1.$$

Here $U_n(t)$ is a Chebyshev polynomial of the second kind, defined by

$$U_n(t)=\frac{\sin((n+1)\theta)}{\sin\theta},\text{ where } t=\cos\theta.$$

## 3. Numerical results

Stress intensity factor (SIF) for the crack tips $A_j$ and $B_j$ of $j$th crack are defined as

$$\begin{aligned}K_{A_j}=(K_1-iK_2)_{A_j}&=\sqrt{2\pi}\lim_{t\to t_{A_j}}\sqrt{|t-t_{A_j}|}g_1'(t),\quad j=1,2\\&=\sqrt{a\pi}F_{A_j}\end{aligned} \tag{19}$$

$$\begin{aligned}K_{B_j}=(K_1-iK_2)_{B_j}&=\sqrt{2\pi}\lim_{t\to t_{B_j}}\sqrt{|t-t_{B_j}|}g_2'(t),\quad j=1,2\\&=\sqrt{b\pi}F_{B_j}\end{aligned} \tag{20}$$

where $F_{A_j}=F_{1A_j}+iF_{2A_j}$ and $F_{B_j}=F_{1B_j}+iF_{2B_j}$ are the nondimensional SIF at cracks tips $A_j$ and $B_j$, respectively.

Consider two inclined cracks with length $2R$ (Fig. 2(a)) and two circular arc cracks with radius $R_1$ and $R_2$ (Fig. 2(b)) in the upper half of bonded dissimilar materials subjected to remote stress $\sigma_{x_1}=\sigma_{x_2}=p$, with the distance between the cracks $d$, the distance between the crack and the boundary $h$ and the bonded materials interface $L_b$.

Table 1 shows the nondimensional SIF for two inclined cracks in bonded dissimilar materials with $\alpha_1=\alpha_2=90^\circ$, $2R/h=1.8$ and different values of $G_2/G_1$ and $2R/d$ (Fig. 2(a)). The nondimensional SIF at cracks tips $A_1$ and $A_2$ equal to SIF at tips $B_1$ and $B_2$, respectively. For $G_1=G_2$, our results are in good agreement with those of Denda and Dong [29] and Murakami [30]. When the distance between two cracks decreases and $G_2/G_1$ increases, the nondimensional SIF decreases at all cracks tips. Table 2 displays the nondimensional SIF for $d/R=1.0$ and $h/R$ varies, our results agree with those of Chen [6] for $G_2=0$. In computation, $M=15$ is chosen and it is enough to archive the required convergence, as compared to Chen [6], $M=25$. It is found that for $G_2/G_1=1.0$ the nondimensional SIF at the cracks tips does not change as $h/R$ varies due to the fact that the plane is made up from one material only. Whereas for $G_2/G_1<1.0$ the nondimensional SIF decreases and for $G_2/G_1>1.0$ the nondimensional SIF increases. Table 3 presents the nondimensional SIF for $\alpha_2=90^\circ$, $d=h$ and $\alpha_1=45^\circ$, and $\alpha_1=90^\circ$. Our results are comparable with those of Chen [10]. Fig. 3 shows the nondimensional SIF against $\alpha_1$ for $\alpha_2=90^\circ$, $d=2h$ and $2R/h=1.8$. It is observed that the Mode I nondimensional SIFs, $F_1$, increases at crack tips $A_1$ and $A_2$ as $\alpha_1$ increases whereas at crack tips $B_1$ and $B_2$, decreases. As $G_2/G_1$ increases, $F_1$ decreases at all cracks tips. The Mode II nondimensional SIF, $F_2$, decreases at crack tips $A_1$ and $A_2$ for $\alpha_1<50^\circ$, whereas at crack tips $B_1$ and $B_2$, $F_2$ does not show any significant differences as $\alpha_1$ increases. Fig. 4 shows the nondimensional SIF for $d=2h$, $2R/h=1.8$ and $\alpha_1=\alpha_2$ varies. It is found that when $\alpha_1=\alpha_2$ increases $F_1$ increases at all cracks tips, and as the ratio $G_2/G_1$ increases $F_1$ decreases. Whereas for Mode II, it is observed that $F_2$ increases at all cracks tips for $\alpha_1=\alpha_2>45^\circ$. As $G_2/G_1$ increases $F_2$ increases at cracks tips $A_1$, $B_1$ and $B_2$, but $F_2$ does not show any significant differences at crack tip $A_2$.

The nondimensional SIF for two circular arc cracks facing the same direction in the upper half of bonded dissimilar materials with $20R_1=9d$, $2R_1=9h$ and subjected to the remote tension $\sigma_x^\infty=\sigma_y^\infty=p$ (Fig. 2(b)) are tabulated in Table 4.

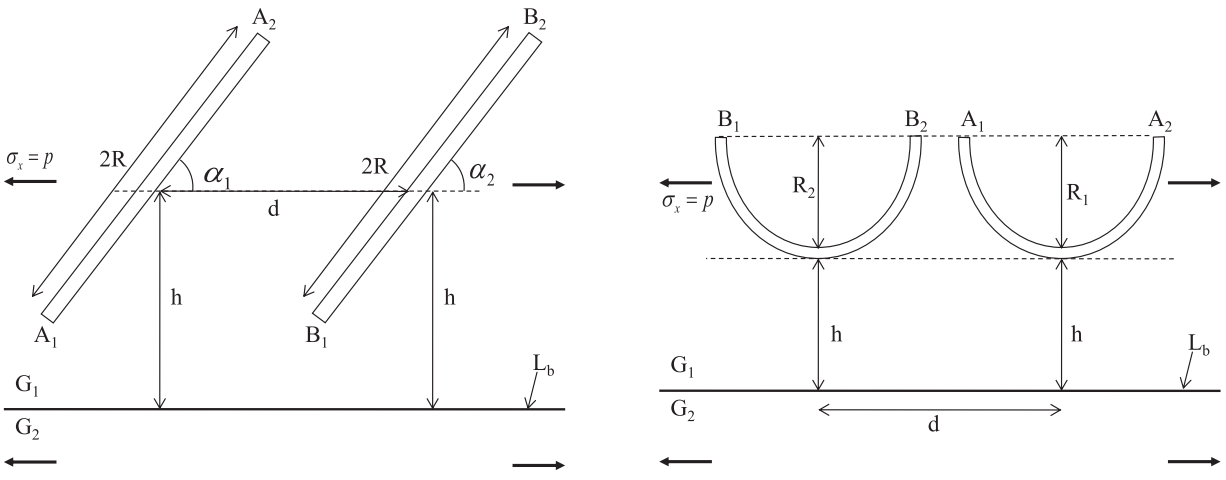


**Fig. 2.** Cracks in the upper half of bonded dissimilar materials: (a) two inclined cracks and (b) two circular arc cracks.

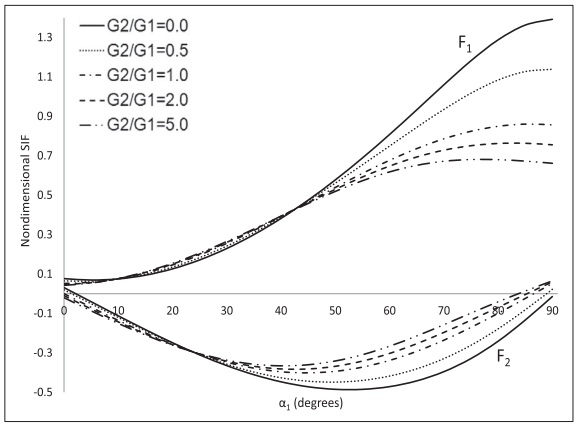


(a) SIF at crack tip $A_1$

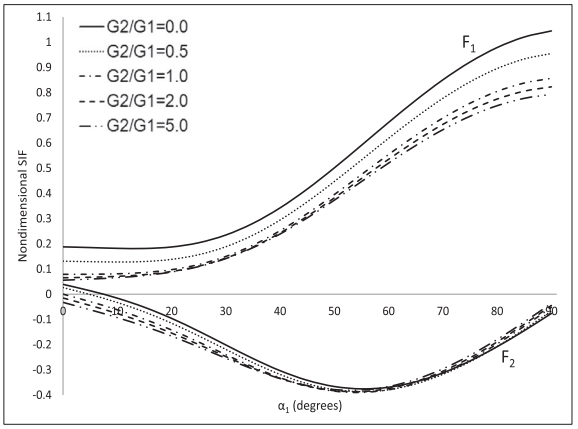


(b) SIF at crack tip $A_2$

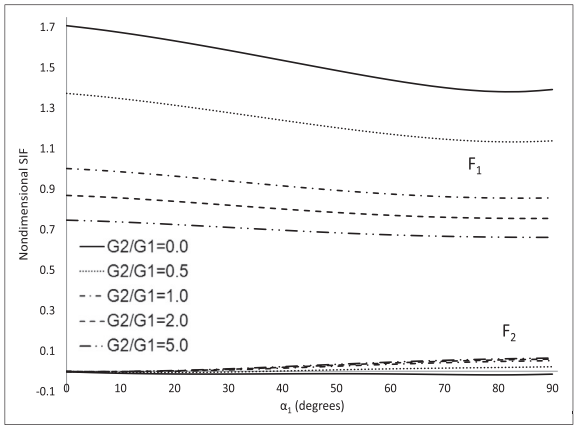


(c) SIF at crack tip $B_1$

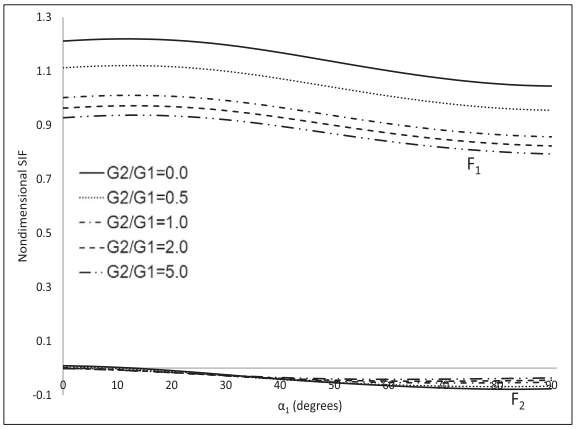


(d) SIF at crack tip $B_2$

**Fig. 3.** Nondimensional SIF at crack tips when $\alpha_1$ is changing for $\alpha_2 = 90^\circ$, $d = 2h$ and $2R/h = 1.8$ (Fig. 2(a)).

**Table 1**
Nondimensional SIF for two inclined cracks in bonded dissimilar materials when $\alpha_1 = \alpha_2 = 90^\circ$ and $2R/h = 1.8$ (Fig. 2(a)).

| $G_2/G_1$ | SIF | $2R/d$ | | | | | |
|---|---|---|---|---|---|---|---|
| | | 0.2 | 0.4 | 0.8 | 1.0 | 2.0 | 5.0 |
| 0.5 | $F_{1A_1}$ [a] | 1.1338 | 1.0831 | 0.9929 | 0.9638 | 0.9008 | 0.8541 |
| | $F_{1A_2}$ [a] | 1.0265 | 0.9885 | 0.9136 | 0.8844 | 0.8120 | 0.7556 |
| | $F_{2A_1}$ [a] | -0.0001 | 0.0029 | 0.0315 | 0.0502 | 0.1114 | 0.1622 |
| | $F_{2A_2}$ [a] | -0.0037 | -0.0162 | -0.0502 | -0.0683 | -0.1271 | -0.1788 |
| 1.0 | $F_{1A_1}$ [a] | 0.9857 | 0.9505 | 0.8722 | 0.8431 | 0.7734 | 0.7215 |
| | $F_{1A_1}$ [b] | 0.9870 | 0.9517 | 0.8732 | 0.8440 | 0.7746 | 0.7129 |
| | $F_{1A_1}$ [c] | 0.9855 | 0.9508 | 0.8727 | 0.8319 | 0.7569 | 0.6962 |
| | $F_{1A_2}$ [a] | 0.9857 | 0.9505 | 0.8722 | 0.8431 | 0.7734 | 0.7215 |
| | $F_{2A_1}$ [a] | 0.0014 | 0.0094 | 0.0431 | 0.0611 | 0.1165 | 0.1633 |
| | $F_{2A_2}$ [a] | −0.0014 | −0.0094 | −0.0431 | −0.0611 | −0.1165 | −0.1633 |
| 5.0 | $F_{1A_1}$ [a] | 0.7426 | 0.7275 | 0.6744 | 0.6499 | 0.5818 | 0.5238 |
| | $F_{1A_2}$ [a] | 0.9170 | 0.8871 | 0.8081 | 0.7799 | 0.7150 | 0.6685 |
| | $F_{2A_1}$ [a] | 0.0026 | 0.0152 | 0.0555 | 0.0742 | 0.1277 | 0.1717 |
| | $F_{2A_2}$ [a] | 0.0016 | 0.0006 | −0.0279 | −0.0443 | −0.0932 | −0.1347 |

[a] Present study.
[b] [29].
[c] [30].

**Table 2**
Nondimensional SIF at crack tips when $h/R$ is changing for $\alpha_1 = \alpha_2 = 90^\circ$ and $d/R = 1.0$ (Fig. 2(a)).

| $G_2/G_1$ | M | SIF | $h/R$ | | | | | | |
|---|---|---|---|---|---|---|---|---|---|
| | | | 0.1 | 0.2 | 0.3 | 0.4 | 0.5 | 0.6 | 0.7 |
| 0.0 | 15 | $F_{1A_1}$ [a] | 1.4174 | 1.2119 | 1.0980 | 1.0228 | 0.9716 | 0.9358 | 0.9099 |
| | 25 | $F_{1A_1}$ [b] | 1.4174 | 1.2119 | 1.0980 | 1.0228 | 0.9716 | 0.9358 | 0.9099 |
| | 15 | $F_{1A_2}$ [a] | 0.9623 | 0.9201 | 0.8923 | 0.8728 | 0.8586 | 0.8478 | 0.8393 |
| | 25 | $F_{1A_2}$ [b] | 0.9623 | 0.9201 | 0.8923 | 0.8728 | 0.8586 | 0.8478 | 0.8393 |
| | 15 | $F_{2A_1}$ [a] | 0.1049 | 0.1212 | 0.1216 | 0.1159 | 0.1101 | 0.1062 | 0.1042 |
| | 25 | $F_{2A_1}$ [b] | 0.1049 | 0.1212 | 0.1216 | 0.1159 | 0.1101 | 0.1062 | 0.1042 |
| | 15 | $F_{2A_2}$ [a] | −0.1484 | −0.1450 | −0.1444 | −0.1438 | −0.1429 | −0.1416 | −0.1400 |
| | 25 | $F_{2A_2}$ [b] | −0.1484 | −0.1450 | −0.1444 | −0.1438 | −0.1429 | −0.1416 | −0.1400 |
| 1.0 | 15 | $F_{1A_1}$ [a] | 0.7734 | 0.7734 | 0.7734 | 0.7734 | 0.7734 | 0.7734 | 0.7734 |
| | 15 | $F_{1A_2}$ [a] | 0.7734 | 0.7734 | 0.7734 | 0.7734 | 0.7734 | 0.7734 | 0.7734 |
| | 15 | $F_{2A_1}$ [a] | 0.1165 | 0.1165 | 0.1165 | 0.1165 | 0.1165 | 0.1165 | 0.1165 |
| | 15 | $F_{2A_2}$ [a] | −0.1165 | −0.1165 | −0.1165 | −0.1165 | −0.1165 | −0.1165 | −0.1165 |
| 5.0 | 15 | $F_{1A_1}$ [a] | 0.5748 | 0.6213 | 0.6498 | 0.6708 | 0.6867 | 0.6991 | 0.7087 |
| | 15 | $F_{1A_2}$ [a] | 0.7142 | 0.7211 | 0.7270 | 0.7318 | 0.7359 | 0.7395 | 0.7424 |
| | 15 | $F_{2A_1}$ [a] | 0.1269 | 0.1300 | 0.1295 | 0.1289 | 0.1284 | 0.1278 | 0.1270 |
| | 15 | $F_{2A_2}$ [a] | −0.0929 | −0.0951 | −0.0969 | −0.0984 | −0.0999 | −0.1013 | −0.1025 |

[a] Present study.
[b] [6].

Our results agree with those of Rafar et al. [4] for the case $G_1 = G_2$. Fig. 5 shows the nondimensional SIF at all cracks tips for $\sigma_x = p$. It is found that at $A_1$ as $R_2/R_1$ and $G_2/G_1$ increase $F_1$ decreases and $F_2$ increases (Fig. 5(a)). At $A_2$, as $R_2/R_1$ increases both $F_1$ and $F_2$ give no significant different but $F_1$ and $F_2$ decreases as $G_2/G_1$ increases (Fig. 5(b)). At $B_1$, as $R_2/R_1$ increases $F_1$ increases and $F_2$ decreases but as $G_2/G_1$ increases $F_1$ decreases and $F_2$ increases. Whereas at $B_2$, as $R_2/R_1$ increases $F_1$ decreases for $R_2/R_1 < 0.8$ and increases for $R_2/R_1 > 0.8$, and $F_2$ decreases. As $G_2/G_1$ increases $F_1$ increases for $R_2/R_1 < 0.8$ and $F_2$ decreases. Fig. 6 exhibits the behaviour of the nondimensional SIF as $h$ varies. At $A_1$ as $h$ increases $F_1$ decreases for $G_2/G_1 < 1.0$ and increases for $G_2/G_1 > 1.0$, and opposite behaviour for $F_2$. At $A_2$ $F_1$ and $F_2$ behave as $F_1$ at $A_1$.

Consider two circular arc cracks, facing in the opposite direction with radius $R$ (Fig. 7(a)) and a semi annulus cracks with radius $R$ and $2R$ (Fig. 7(b)), in the upper half of bonded dissimilar materials subjected to remote stress $\sigma_{x_1} = \sigma_{x_2} = p$. $d$, $h$ and $L_b$ are explained in Fig. 7.

Tables 5 and 6 display the nondimensional SIF at cracks tips for $F_1$ and $F_2$, respectively. For $G_1 = G_2$, as $h/R$ increases both $F_1$ and $F_2$ remains constant, for $G_2/G_1 < 1.0$ $F_1$ decreases and for $G_2/G_1 > 1.0$ $F_1$ increases.

Fig. 8 shows the nondimensional SIF when $\alpha$ is changing for $h = 0.5R$ as defined in Fig. 7(b). It is found that $F_1$ at cracks tips $A_1$ and $B_1$ equals to $F_1$ at tips $A_2$ and $B_2$, respectively. At crack tips $A_1$ and $B_1$, as $\alpha$ and $G_2/G_1$ increase $F_1$ increases and decreases, respectively. Whereas $F_2$ at cracks tips $A_1$ and $B_1$ equal to negative of $F_2$ at tips $A_2$ and $B_2$, respectively. At crack tips $A_1$ and $B_1$, $F_2$ decreases for the angle $\alpha > 50^\circ$ and increases as $G_2/G_1$ increases.

**Table 3**
Nondimensional SIF at crack tips when $\alpha_1$ is changing for $\alpha_2 = 90^\circ$, $d = h$ and $2R/h = 1.8$ (Fig. 2(a)).

| SIF | $G_2/G_1$ | | | | | |
|---|---|---|---|---|---|---|
| | $\alpha_1 = 45^\circ$ | | | $\alpha_1 = 90^\circ$ | | |
| | 0.2 | 1.0 | 5.0 | 0.2 | 1.0 | 5.0 |
| $F_{1A_1}$ [a] | 0.4634 | 0.4250 | 0.4219 | 1.0858 | 0.7818 | 0.5908 |
| $F_{1A_1}$ [b] | 0.4670 | 0.4250 | 0.4020 | 1.0310 | 0.7820 | 0.6070 |
| $F_{1A_2}$ [a] | 0.0612 | 0.0420 | 0.0571 | 0.8760 | 0.7818 | 0.7226 |
| $F_{1A_2}$ [b] | 0.0420 | 0.0420 | 0.0370 | 0.8590 | 0.7820 | 0.7280 |
| $F_{2A_1}$ [a] | −0.3358 | −0.3226 | −0.3000 | 0.0973 | 0.1092 | 0.1208 |
| $F_{2A_1}$ [b] | −0.3330 | −0.3230 | −0.2830 | 0.0940 | 0.1090 | 0.1230 |
| $F_{2A_2}$ [a] | −0.1974 | −0.2341 | −0.2352 | −0.1287 | −0.1092 | −0.0868 |
| $F_{2A_2}$ [b] | −0.2010 | −0.2360 | −0.2400 | −0.1340 | −0.1090 | −0.0840 |
| $F_{1B_1}$ [a] | 1.2272 | 0.8909 | 0.6666 | 1.0858 | 0.7818 | 0.5908 |
| $F_{1B_1}$ [b] | 1.2140 | 0.8910 | 0.6600 | 1.0310 | 0.7820 | 0.6070 |
| $F_{1B_2}$ [a] | 1.1004 | 0.9844 | 0.9128 | 0.8760 | 0.7818 | 0.7226 |
| $F_{1B_2}$ [b] | 1.1010 | 0.9850 | 0.9030 | 0.8590 | 0.7820 | 0.7280 |
| $F_{2B_1}$ [a] | 0.0336 | 0.0364 | 0.0486 | 0.0973 | −0.1092 | 0.1208 |
| $F_{2B_1}$ [b] | 0.0180 | 0.0360 | 0.0440 | 0.0940 | −0.1090 | 0.1230 |
| $F_{2B_2}$ [a] | −0.0510 | −0.0536 | −0.0472 | −0.1287 | −0.1092 | −0.0868 |
| $F_{2B_2}$ [b] | −0.0650 | −0.0530 | −0.0460 | −0.1340 | −0.1090 | −0.0840 |

[a] Present study.
[b] [10].

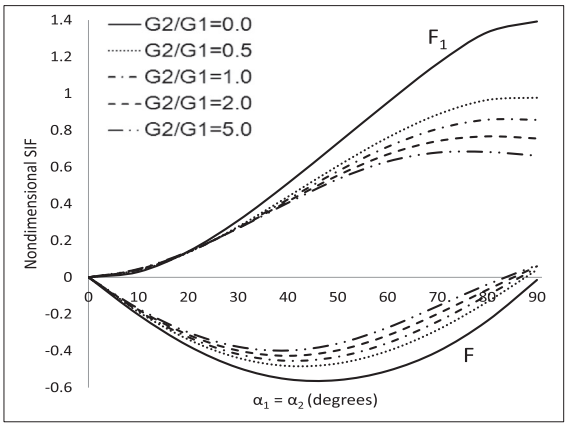


(a) SIF at crack tip $A_1$

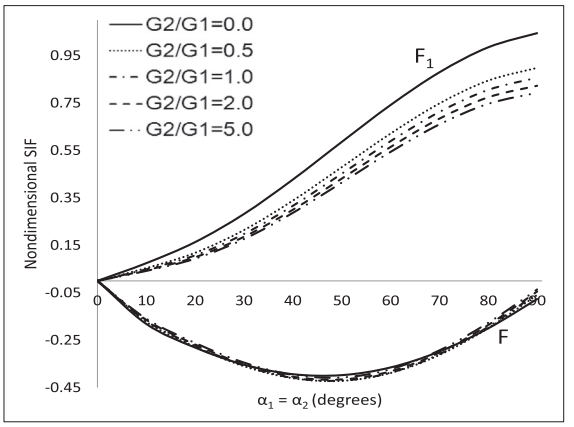


(b) SIF at crack tip $A_2$

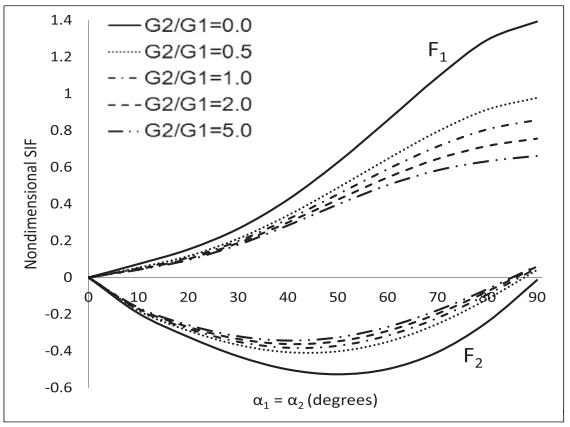


(c) SIF at crack tip $B_1$

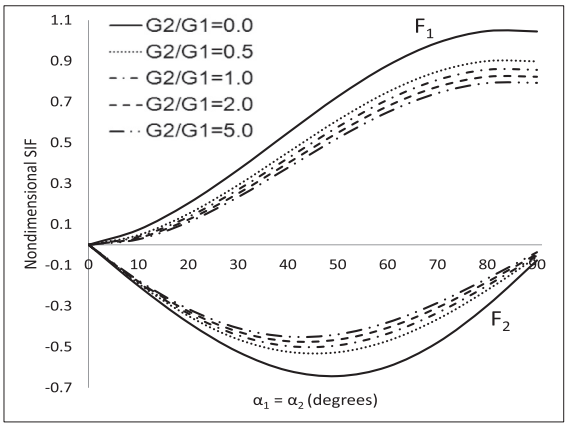


(d) SIF at crack tip $B_2$

**Fig. 4.** Nondimensional SIF at crack tips when $\alpha_1 = \alpha_2$ is changing for $d = 2h$ and $2R/h = 1.8$ (Fig. 2(a)).

**Table 4**
Nondimensional SIF for two circular arc cracks in bonded dissimilar materials for the case $G_1 = G_2$, when $20R_1 = 9d$ and $2R_1 = 9h$ (Fig. 2(b)).

| SIF | $R_2/R_1$ | | | | | | | |
|---|---|---|---|---|---|---|---|---|
| | 0.1 | 0.2 | 0.3 | 0.4 | 0.5 | 0.6 | 0.7 | 1.0 |
| $F_{1A_1}$ [a] | 0.3753 | 0.3724 | 0.3684 | 0.3640 | 0.3602 | 0.3579 | 0.3576 | 0.3295 |
| $F_{1A_1}$ [b] | 0.3753 | 0.3725 | 0.3685 | 0.3643 | 0.3605 | 0.3582 | 0.3580 | 0.3297 |
| $F_{1A_2}$ [a] | 0.3764 | 0.3764 | 0.3763 | 0.3763 | 0.3765 | 0.3772 | 0.3786 | 0.3946 |
| $F_{1A_2}$ [b] | 0.3764 | 0.3764 | 0.3763 | 0.3763 | 0.3764 | 0.3770 | 0.3785 | 0.3949 |
| $F_{2A_1}$ [a] | −0.3776 | −0.3798 | −0.3842 | −0.3915 | −0.4022 | −0.4172 | −0.4369 | −0.5337 |
| $F_{2A_1}$ [b] | −0.3776 | −0.3797 | −0.3840 | −0.3912 | −0.4017 | −0.4163 | −0.4358 | −0.5316 |
| $F_{2A_2}$ [a] | 0.3774 | 0.3787 | 0.3808 | 0.3840 | 0.3884 | 0.3939 | 0.4007 | 0.4338 |
| $F_{2A_2}$ [b] | 0.3775 | 0.3788 | 0.3809 | 0.3840 | 0.3882 | 0.3936 | 0.4003 | 0.4324 |
| $F_{1B_1}$ [a] | 0.3007 | 0.3144 | 0.3275 | 0.3399 | 0.3515 | 0.3621 | 0.3716 | 0.3946 |
| $F_{1B_1}$ [b] | 0.3030 | 0.3165 | 0.3294 | 0.3416 | 0.3529 | 0.3632 | 0.3726 | 0.3949 |
| $F_{1B_2}$ [a] | 0.3293 | 0.3172 | 0.3044 | 0.2910 | 0.2774 | 0.2644 | 0.2540 | 0.3295 |
| $F_{1B_2}$ [b] | 0.3286 | 0.3166 | 0.3039 | 0.2908 | 0.2772 | 0.2642 | 0.2539 | 0.3297 |
| $F_{2B_1}$ [a] | −0.4404 | −0.4434 | −0.4444 | −0.4438 | −0.4428 | −0.4407 | −0.4383 | −0.4337 |
| $F_{2B_1}$ [b] | −0.4386 | −0.4415 | −0.4425 | −0.4421 | −0.4410 | −0.4388 | −0.4365 | −0.4324 |
| $F_{2B_2}$ [a] | 0.4601 | 0.4667 | 0.4736 | 0.4803 | 0.4870 | 0.4934 | 0.4990 | 0.5337 |
| $F_{2B_2}$ [b] | 0.4598 | 0.4663 | 0.4729 | 0.4798 | 0.4863 | 0.4923 | 0.4978 | 0.5316 |

[a] Present study.
[b] [4].

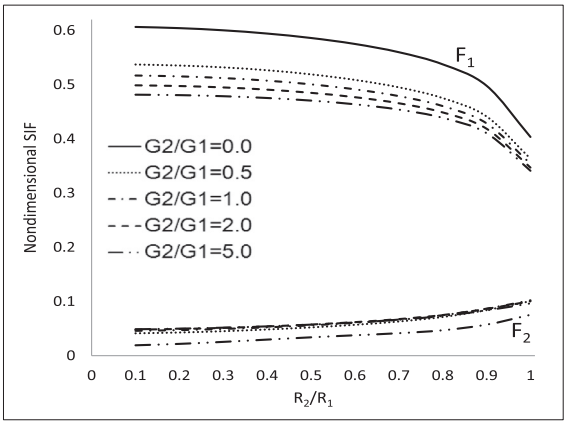


(a) SIF at crack tip $A_1$

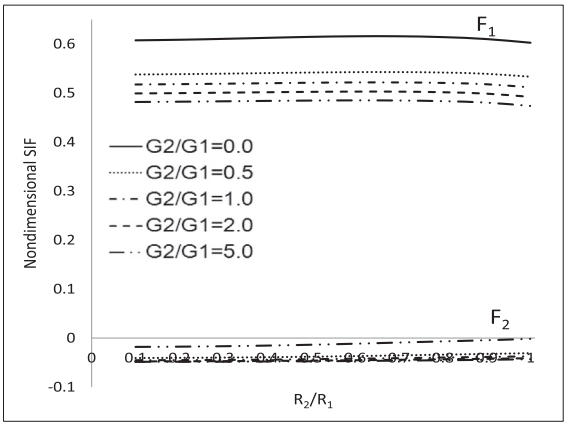


(b) SIF at crack tip $A_2$

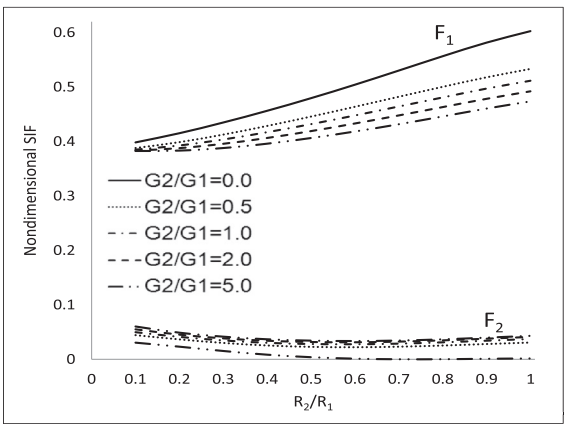


(c) SIF at crack tip $B_1$

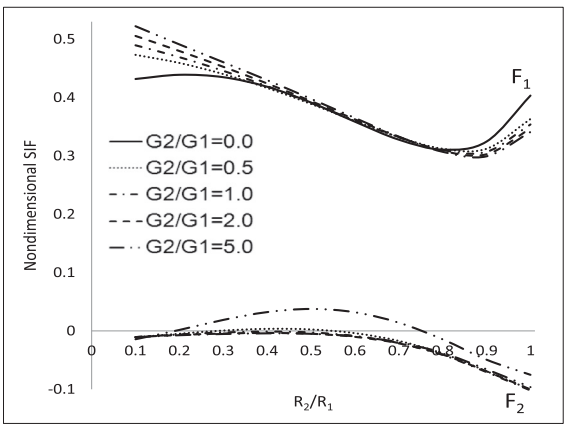


(d) SIF at crack tip $B_2$

**Fig. 5.** Nondimensional SIF for two circular arc cracks subjected to the remote tension $\sigma_x = p$ (Fig. 2(b)).

**Table 5**
Nondimensional SIF, $F_1$, for two circular arc cracks facing in the opposite direction in the upper half of bonded dissimilar materials (Fig. 7(a)).

| $G_2/G_1$ | SIF | $h/R$ | | | | | | |
|---|---|---|---|---|---|---|---|---|
| | | 0.2 | 0.4 | 0.6 | 0.8 | 1.0 | 1.2 | 1.4 |
| 0.0 | $F_{1A_1}$ | 0.5994 | 0.5666 | 0.5454 | 0.5295 | 0.5191 | 0.5125 | 0.5086 |
| | $F_{1A_2}$ | 0.6033 | 0.5792 | 0.5651 | 0.5554 | 0.5485 | 0.5435 | 0.5398 |
| | $F_{1B_1}$ | 0.9214 | 0.9315 | 0.9308 | 0.9291 | 0.9269 | 0.9246 | 0.9224 |
| | $F_{1B_2}$ | 0.8499 | 0.8375 | 0.8239 | 0.8151 | 0.8089 | 0.8042 | 0.8008 |
| 0.5 | $F_{1A_1}$ | 0.5214 | 0.5131 | 0.5080 | 0.5046 | 0.5022 | 0.5005 | 0.4995 |
| | $F_{1A_2}$ | 0.5463 | 0.5376 | 0.5339 | 0.5315 | 0.5297 | 0.5284 | 0.5275 |
| | $F_{1B_1}$ | 0.9139 | 0.9139 | 0.9137 | 0.9133 | 0.9130 | 0.9125 | 0.9121 |
| | $F_{1B_2}$ | 0.7999 | 0.7957 | 0.7931 | 0.7911 | 0.7896 | 0.7885 | 0.7876 |
| 1.0 | $F_{1A_1}$ | 0.4954 | 0.4954 | 0.4954 | 0.4954 | 0.4954 | 0.4954 | 0.4954 |
| | $F_{1A_2}$ | 0.5228 | 0.5228 | 0.5228 | 0.5228 | 0.5228 | 0.5228 | 0.5228 |
| | $F_{1B_1}$ | 0.9085 | 0.9085 | 0.9085 | 0.9085 | 0.9085 | 0.9085 | 0.9085 |
| | $F_{1B_2}$ | 0.7822 | 0.7822 | 0.7822 | 0.7822 | 0.7822 | 0.7822 | 0.7822 |
| 2.0 | $F_{1A_1}$ | 0.4713 | 0.4794 | 0.4837 | 0.4866 | 0.4887 | 0.4901 | 0.4911 |
| | $F_{1A_2}$ | 0.4990 | 0.5086 | 0.5124 | 0.5148 | 0.5164 | 0.5175 | 0.5184 |
| | $F_{1B_1}$ | 0.9048 | 0.9045 | 0.9045 | 0.9046 | 0.9049 | 0.9051 | 0.9054 |
| | $F_{1B_2}$ | 0.7670 | 0.7698 | 0.7720 | 0.7736 | 0.7750 | 0.7760 | 0.7769 |
| 5.0 | $F_{1A_1}$ | 0.4468 | 0.4638 | 0.4720 | 0.4777 | 0.4816 | 0.4843 | 0.4863 |
| | $F_{1A_2}$ | 0.4732 | 0.4935 | 0.5017 | 0.5065 | 0.5098 | 0.5121 | 0.5139 |
| | $F_{1B_1}$ | 0.9019 | 0.9013 | 0.9011 | 0.9012 | 0.9015 | 0.9019 | 0.9025 |
| | $F_{1B_2}$ | 0.7527 | 0.7577 | 0.7616 | 0.7648 | 0.7674 | 0.7695 | 0.7712 |

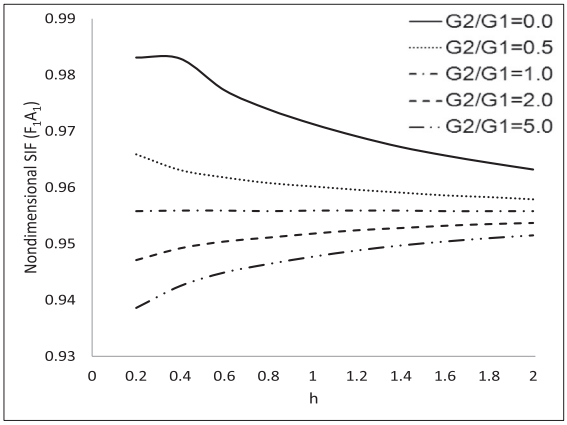


(a) SIF, $F_1$, at crack tip $A_1$

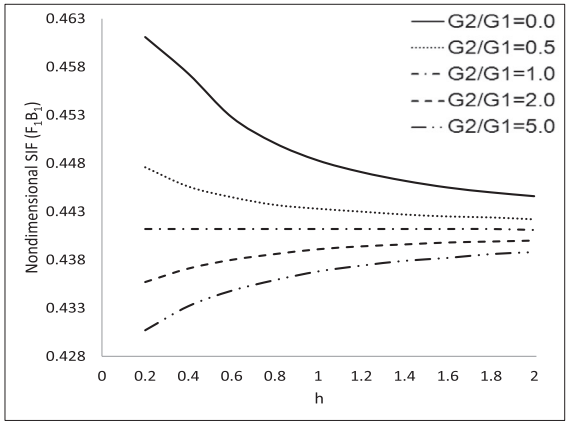


(b) SIF, $F_1$, at crack tip $A_2$

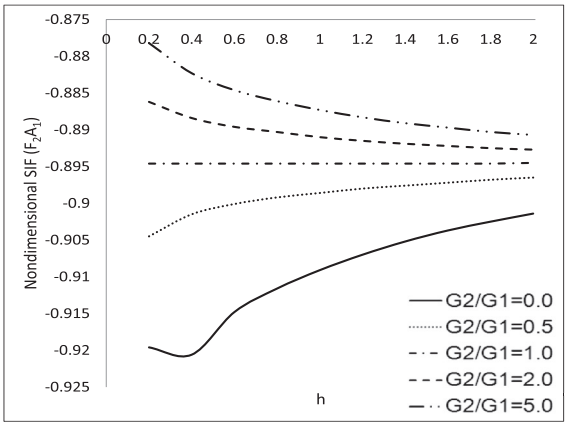


(c) SIF, $F_2$, at crack tip $A_1$

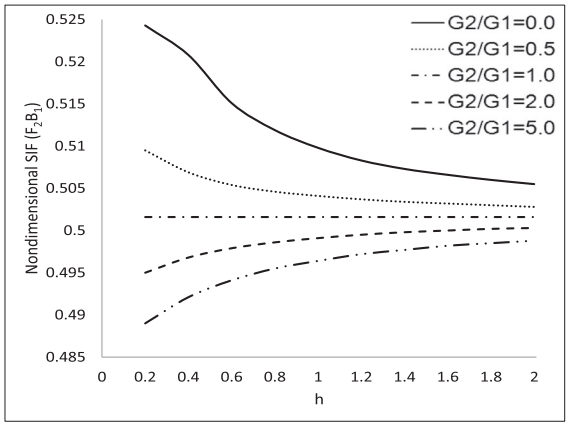


(d) SIF, $F_2$, at crack tip $A_2$

**Fig. 6.** Nondimensional SIF when $h$ is changing for $R_1 = R_2$ and $9d = 20R_1$ (Fig. 2(b)).

**Table 6**
Nondimensional SIF, $F_2$, for two circular arc cracks facing in the opposite direction in the upper half of bonded dissimilar materials (Fig. 7(a)).

| $G_2/G_1$ | SIF | $h/R$ | | | | | | |
|---|---|---|---|---|---|---|---|---|
| | | 0.2 | 0.4 | 0.6 | 0.8 | 1.0 | 1.2 | 1.4 |
| 0.0 | $F_{2A_1}$ | 0.0033 | 0.0170 | 0.0278 | 0.0361 | 0.0423 | 0.0467 | 0.0497 |
| | $F_{2A_2}$ | 0.0006 | −0.0105 | −0.0202 | −0.0279 | −0.0333 | -0.0368 | -0.0390 |
| | $F_{2B_1}$ | −0.8529 | −0.8648 | −0.8646 | −0.8632 | −0.8613 | −0.8592 | −0.8571 |
| | $F_{2B_2}$ | 0.8206 | 0.8079 | 0.7934 | 0.7843 | 0.7780 | 0.7734 | 0.7700 |
| 0.5 | $F_{2A_1}$ | 0.0560 | 0.0529 | 0.0520 | 0.0521 | 0.0526 | 0.0531 | 0.0534 |
| | $F_{2A_2}$ | −0.0452 | −0.0414 | −0.0402 | −0.0402 | −0.0404 | −0.0407 | −0.0409 |
| | $F_{2B_1}$ | −0.8493 | −0.8492 | −0.8491 | −0.8488 | −0.8485 | −0.8481 | −0.8478 |
| | $F_{2B_2}$ | 0.7708 | 0.7659 | 0.7628 | 0.7606 | 0.7591 | 0.7579 | 0.7570 |
| 1.0 | $F_{2A_1}$ | 0.0532 | 0.0532 | 0.0532 | 0.0532 | 0.0532 | 0.0532 | 0.0532 |
| | $F_{2A_2}$ | −0.0400 | −0.0400 | −0.0400 | −0.0400 | −0.0400 | −0.0400 | −0.0400 |
| | $F_{2B_1}$ | −0.8447 | −0.8447 | −0.8447 | −0.8447 | −0.8447 | −0.8447 | −0.8447 |
| | $F_{2B_2}$ | 0.7516 | 0.7516 | 0.7516 | 0.7516 | 0.7516 | 0.7516 | 0.7516 |
| 2.0 | $F_{2A_1}$ | 0.0482 | 0.0508 | 0.0520 | 0.0523 | 0.0523 | 0.0522 | 0.0521 |
| | $F_{2A_2}$ | −0.0328 | −0.0360 | −0.0375 | −0.0380 | −0.0382 | −0.0383 | −0.0384 |
| | $F_{2B_1}$ | −0.8420 | −0.8417 | −0.8416 | −0.8416 | −0.8418 | −0.8420 | −0.8422 |
| | $F_{2B_2}$ | 0.7350 | 0.7385 | 0.7410 | 0.7428 | 0.7442 | 0.7453 | 0.7462 |
| 5.0 | $F_{2A_1}$ | 0.0422 | 0.0467 | 0.0490 | 0.0499 | 0.0501 | 0.0501 | 0.0501 |
| | $F_{2A_2}$ | −0.0248 | −0.0303 | −0.0332 | −0.0345 | −0.0351 | −0.0355 | −0.0358 |
| | $F_{2B_1}$ | −0.8403 | −0.8397 | −0.8394 | −0.8392 | −0.8393 | −0.8396 | −0.8399 |
| | $F_{2B_2}$ | 0.7192 | 0.7254 | 0.7301 | 0.7336 | 0.7364 | 0.7386 | 0.7404 |

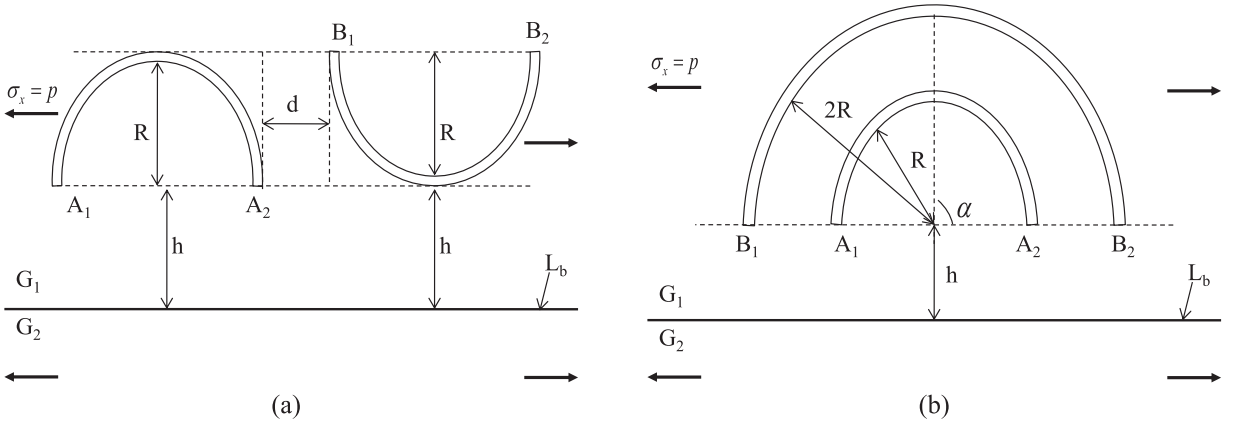


**Fig. 7.** Double circular arc cracks in the upper half of bonded dissimilar materials.

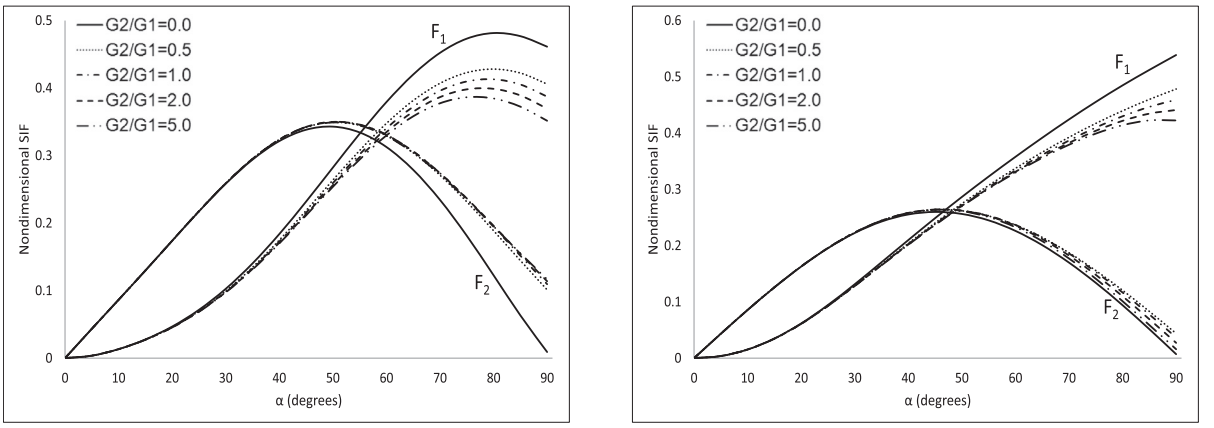


**Fig. 8.** Nondimensional SIF for a semi annulus crack when $\alpha$ is changing for $h = 0.5R$ (Fig. 7(b)).

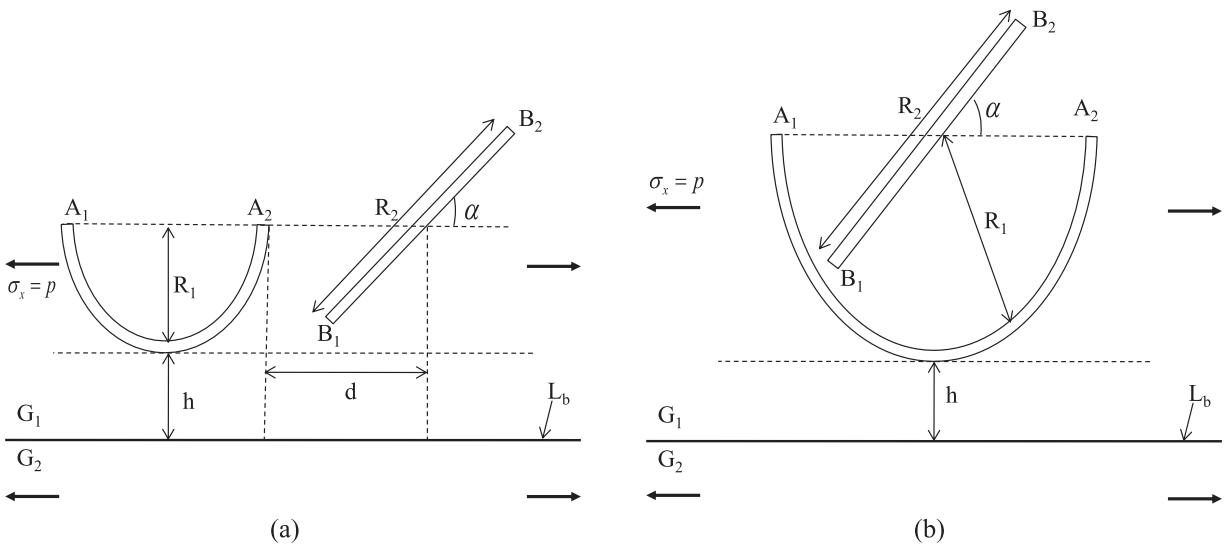


**Fig. 9.** An inclined and a semi circular arc cracks in the upper half of bonded dissimilar materials.

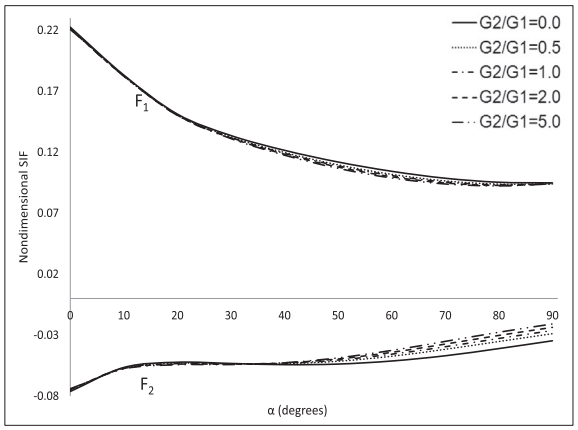


(a) SIF at crack tip $A_1$

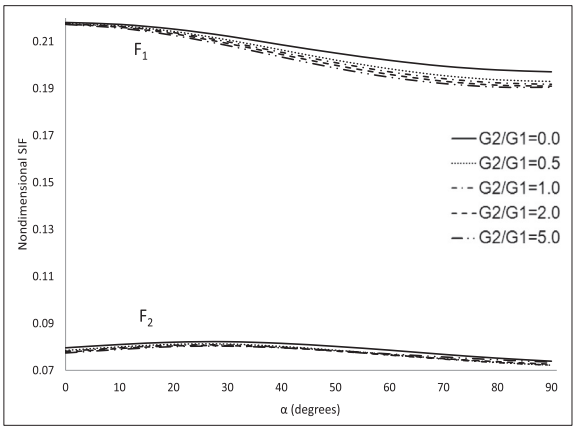


(b) SIF at crack tip $A_2$

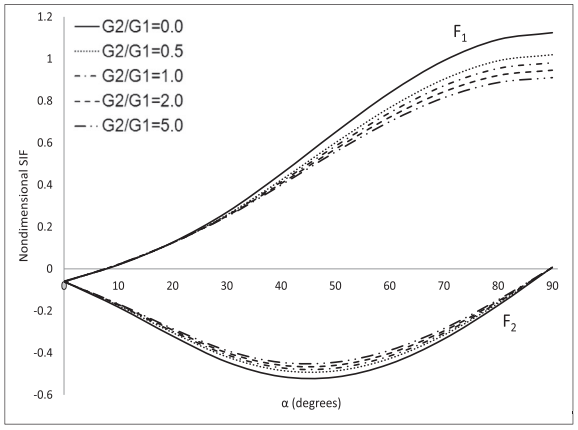


(c) SIF at crack tip $B_1$

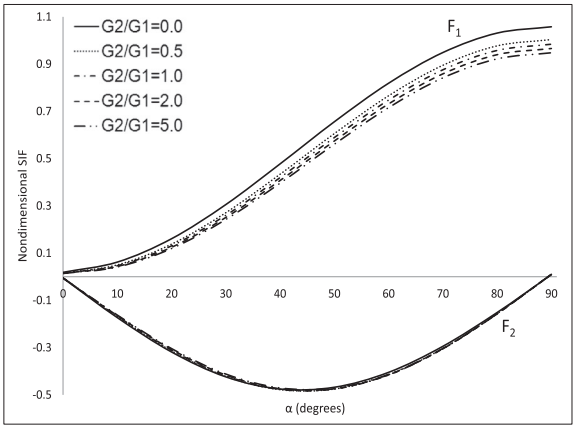


(d) SIF at crack tip $B_2$

**Fig. 10.** Nondimensional SIF for an inclined crack is located on the right position of the semi circular arc crack in bonded dissimilar materials (Fig. 9(a)).

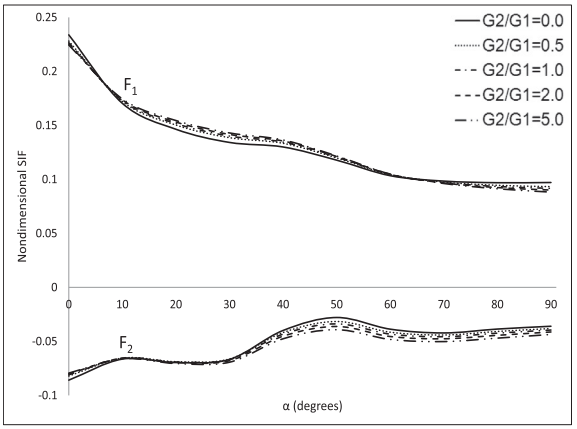


(a) SIF at crack tip $A_1$

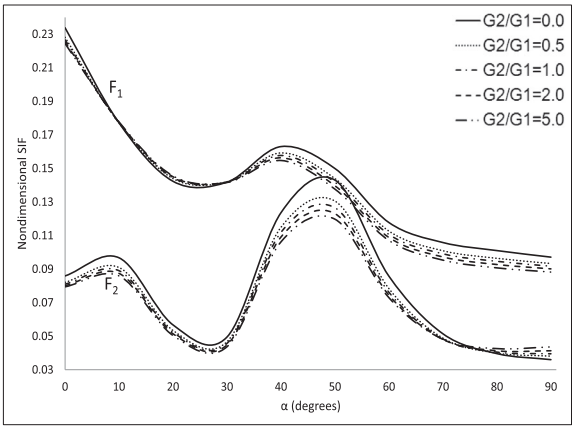


(b) SIF at crack tip $A_2$

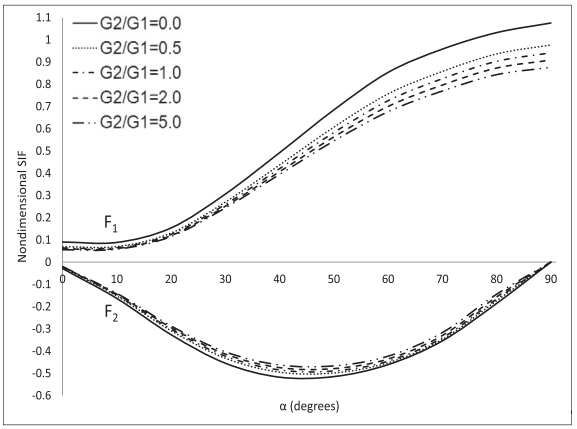


(c) SIF at crack tip $B_1$

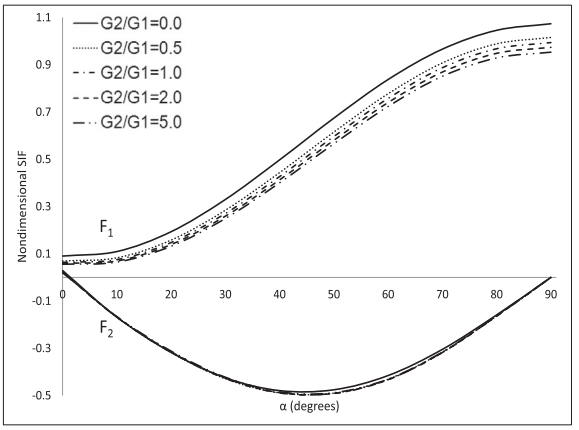


(d) SIF at crack tip $B_2$

**Fig. 11.** Nondimensional SIF for an inclined crack is located on the upper position of the semi circular arc crack in bonded dissimilar materials (Fig. 9(b)).

Consider an inclined and a circular arc cracks in the upper half of bonded dissimilar materials subjected to remote stress $\sigma_{x_1} = \sigma_{x_2} = p$ as in Fig. 9. Fig. 10 shows the nondimensional SIF for $d = R_1$, $R_1 = 2h$, $R_2 = 1.8R_1$ and $\alpha$ varies as defined in Fig. 9(a). It is found that at $A_1$ as $\alpha$ and $G_2/G_1$ increase $F_1$ decreases and $F_2$ increases. At $A_2$ as $\alpha$ and $G_2/G_1$ increase $F_1$ decreases and $F_2$ does not show any significance differences. At $B_1$ as $\alpha$ increases $F_1$ increases and $F_2$ increases for $\alpha > 40^\circ$. As $G_2/G_1$ increases $F_1$ decreases and $F_2$ increases. Whereas at $B_2$ as $\alpha$ increases $F_1$ increases and $F_2$ increases for $\alpha > 40^\circ$. As $G_2/G_1$ increases $F_1$ decreases and $F_2$ does not show any significant differences. Fig. 11 shows the nondimensional SIF, $F_1$ and $F_2$ for cracks defined in Fig. 9(b). It is found that at $A_1$ as $\alpha$ increases $F_1$ decreases and $F_2$ increases, and as $G_2/G_1$ increases $F_1$ increases for $10 < \alpha < 60$ and $F_2$ decreases. At $A_2$ as $\alpha$ increases $F_1$ decreases, and as $G_2/G_1$ increases $F_1$ and $F_2$ decrease. At $B_1$ as $\alpha$ increases $F_1$ increases and $F_2$ increases for $\alpha > 40^\circ$, and as $G_2/G_1$ increases $F_1$ decreases and $F_2$ decreases. Whereas at $B_2$ as $\alpha$ increases $F_1$ increases and $F_2$ increases for $\alpha > 40^\circ$, and as $G_2/G_1$ increases $F_1$ decreases and $F_2$ does not show significant differences.

## 4. Conclusions

The new hypersingular integral equations (HSIEs) for the cracks problems in the upper half of bonded dissimilar materials subjected to remote stress is formulated. These equations are solved numerically using the curved length coordinate method and the appropriate quadrature formulas. Our numerical results are accurate, efficient and rapidly convergence as compared to the previous work. To conclude, the elastic constant ratios, the distance between cracks and the distance between crack and the boundary of the materials have strong influences on the Mode I and Mode II nondimensional SIF. However their influence is altered for different crack geometries.

For the cracks problems in both upper and lower planes of the bonded dissimilar materials will be treated later.

## Acknowledgements

The second author thanks the Universiti Putra Malaysia for the Putra Grant, project no: 9567900 and FRGS project no: 01-01-16-18685R5524975.

## References

[1] T. Zheng, Z. Zhu, B. Wang, L. Zeng, Stress intensity factor for an infinite plane containing three collinear cracks under compression, ZAMM J. Appl. Math. Mech. 94 (10) (2014) 853–861.
[2] N.M.A.N. Long, M.R. Aridi, Z.K. Eshkuvatov, Mode stresses for the interaction between an inclined crack and a curved crack in plane elasticity, Math. Probl. Eng. 2015 (2015) 1–10.
[3] M.R. Aridi, N.M.A.N. Long, Z.K. Eshkuvatov, Stress intensity factor for the interaction between a straight crack and a curved crack in plane elasticity, Acta Mech. Solida Sin. 29 (4) (2016) 1–9.
[4] R.A. Rafar, N.M.A.N. Long, N. Senu, N.A. Noda, Stress intensity factor for multiple inclined or curved cracks problem in circular positions in plane elasticity, ZAMM J. Appl. Math. Mech. 97 (11) (2017) 1482–1494.
[5] Y.Z. Chen, X.Y. Lin, X.Z. Wang, Numerical solution for curved crack problem in elastic half-plane using hypersingular integral equation, Philos. Mag. 89 (26) (2009) 2239–2253.
[6] Y.Z. Chen, Evaluation of the t-stress for multiple cracks in an elastic half-plane using singular integral equation and green's function method, Appl. Math. Comput. 228 (2014) 17–30.
[7] N.R.F. Elfakhakhre, N.M.A.N. Long, Z.K. Eshkuvatov, Stress intensity factor for multiple cracks in half plane elasticity, in: AIP Conference Proceedings 1795, 2017, pp. 1–8.
[8] N.R.F. Elfakhakhre, N.M.A.N. Long, Z.K. Eshkuvatov, Stress intensity factor for an elastic half plane weakened by multiple curved cracks, Appl. Math. Model. 60 (2018) 540–551.
[9] H. Ferdjani, R. Abdelmoula, Propagation of a Dugdale crack at the edge of a half plane, Contin. Mech. Thermodyn. 30 (1) (2018) 195–205.
[10] Y.Z. Chen, Multiple crack problems for two bonded half planes in plane and antiplane elasticity, Eng. Fract. Mech. 25 (1) (1986) 1–9.
[11] Y.Z. Chen, N. Hasebe, Stress-intensity factors for curved circular crack in bonded dissimilar materials, Theor. Appl. Fract. Mech. 17 (1992) 189–196.
[12] M. Isida, H. Noguchi, Arbitrary array of cracks in bonded half planes subjected to various loadings, Eng. Fract. Mech. 46 (3) (1993) 365–380.
[13] M. Isida, H. Noguchi, Distributed cracks and kinked cracks in bonded dissimilar half planes with an interface crack, Int. J. Fract. 66 (1994) 313–337.
[14] N. Hasebe, S. Kato, Debonding fracture of bonded bimaterial semistrips subjected to concentrated forces and couples, ZAMM J. Appl. Math. Mech. 96 (6) (2016) 758–772.
[15] X. Lan, S. Ji, N.A. Noda, Y. Cheng, Stress intensity factor solutions for several crack problems using the proportional crack opening displacements, Eng. Fract. Mech. 171 (2017) 35–49.
[16] P.A. Juan, R. Dingreville, Mechanics of finite cracks in dissimilar anisotropic elastic media considering interfacial elasticity, J. Mech. Phys. Solids 99 (2017) 1–18.
[17] Y. Wang, H. Waisman, Material dependent crack-tip enrichment functions in XFEM for modeling interfacial cracks in bimaterials, Int. J. Numer. Methods Eng. 112 (11) (2017) 1495–1518.
[18] Y. Li, E. Viola, Size effect investigation of a central interface crack between two bonded dissimilar materials, Compos. Struct. 105 (2013) 90–107.
[19] R. Ghajar, S. Peyman, J. Sheikhi, M. Poorjamshidian, Numerical inventigation of the mixed-mode stress intensity factors in FGMs considering the effect of graded poisson's ratio, J. Solid Mech. 9 (1) (2017) 172–185.
[20] S. Itou, Stress intensity factors for four interface-close cracks between a nonhomogeneous bonding layer and one of two dissimilar elastic half-planes, Eur. J. Mech. A/Solids 59 (2016) 242–251.
[21] A. Mousavi, M.R.M. Aliha, Determination of fracture parameters for a bi-material center cracked plate subjected to biaxial loading using FEOD method, Eng. Mech. 4 (2016) 117–124.
[22] B. Serier, M. Belhouari, B. Bachir Bouiadjra, Numerical study of the interaction between an interfacial crack and a subinterfacial microcrack in bi-materials, Comput. Mater. Sci. 29 (2004) 309–314.
[23] Y.Z. Chen, N. Hasebe, Properties of eigenfunction expansion form for the rigid line problem in dissimilar media, Int. J. Solids Struct. 33 (5) (1996) 611–628.
[24] X. Han, F. Ellyin, Z. Xia, A crack near the interface of bonded elastic-viscoelastic planes, Int. J. Solids Struct. 38 (2001) 3453–3468.
[25] X. Han, F. Ellyin, Z. Xia, Interaction among interface, multiple cracks and dislocations, Int. J. Solids Struct. 39 (2002) 1575–1590.
[26] N.I. Muskhelishvili, Some Basic Problems of the Mathematical Theory of Elasticity, Noordhoff International Publishing, Leyden, 1953.
[27] M.R. Aridi, N.M.A.N. Long, Z.K. Eshkuvatov, Mode stresses for the interaction between straight and curved cracks problem in plane elasticity, J. Appl. Math. Phys. 2 (2014) 225–234.
[28] N.M.A.N. Long, Z.K. Eshkuvatov, Hypersingular integral equation for multiple curved cracks problem in plane elasticity, Int. J. Solids Struct. 46 (2009) 2611–2617.
[29] M. Denda, Y.F. Dong, Complex variable approach to the BEM for multiple crack problems, Comput. Methods Appl. Mech. Eng. 141 (1997) 247–264.
[30] Y. Murakami, Handbook of Stress Intensity Factors, Pergamon Press, Oxford, 1987.